Synthesis, Mössbauer, cyclic voltammetry, magnetic properties and molecular structures of the low-spin iron(III) bis(pyrazine) complexes with the para-fluoro and para-chloro substituted meso-tetraphenylporphyrin

Selma Dhifaoui, Soumaya Nasri, Geoffrey Gontard, Ashta Ghosh, Yann Garcia, Cecilia Bonifàcio, Shabir Najmudin, Valerie Marvaud, Habib Nasri

Synthesis, Mössbauer, cyclic voltammetry, magnetic properties and molecular structures of the low-spin iron(III) bis(pyrazine) complexes with the *para*-fluoro and *para*-chloro substituted *meso*-tetraphenylporphyrin

Selma Dhifaoui [a], Soumaya Nasri [a], Geoffrey Gontard [b], Ashta C. Ghosh [c], Yann Garcia [c], Cecilia Bonifàcio [d], Shabir Najmudin [e], Valérie Marvaud [b], Habib Nasri [a,*]

[a] University of Monastir, Laboratoire de Physico-chimie des Matériaux, Faculté des Sciences de Monastir, Avenue de L 'environnement, 5019 Monastir, Tunisia
[b] IPCM, Institut Parisien de Chimie Moléculaire, UPMC, Sorbonne Université, 4 Place Jussieu, 75252 Paris Cedex 05, France
[c] Université Catholique de Louvain, Institute of Condensed Matter and Nanosciences, Molecules, Solids and Reactivity (IMCN/MOST), Place L Pasteur 1, 1348 Louvain-la-Neuve, Belgium
[d] REQUIMTE/CQFB Departamento de Quimica, Faculdade de Ciencias e Tecnologia, Universidade Nova de Lisboa, 2829-516 Caparica, Portugal
[e] CIISA – Faculdade de Medicina, Veterinária, Universidade de Lisboa, Avenida da UniversidadeTecnica, 1300-477 Lisboa, Portugal

ARTICLE INFO

Article history:
Received 19 July 2017
Received in revised form 15 February 2018
Accepted 16 February 2018
Available online 17 February 2018

Keywords:
Iron(III) porphyrins
X-ray molecular structure
UV-visible
Mössbauer
Magnetic properties

ABSTRACT

Two new bis(pyrazine) iron(III) *meso*-porphyrin complexes are reported here: the bis(pyrazine) [5,10,15,20-tetra(*para*-fluoro-phenyl)porphyrinato]iron(III) triflate; $[Fe(TFPP)(pyz)_2]SO_3CF_3$ (**1**) and the bis(pyrazine)[5,10,15,20-tetra(*para*-chlorophenyl)porphyrinato]iron(III) triflate; $[Fe(TClPP)(pyz)_2]SO_3CF_3$ (**2**). The X-ray molecular structures of **1**–**2** show that the planes of the two pyrazine axial ligands are perpendicular and that the porphyrin macrocycles of these derivatives are very distorted, leading to a short average equatorial iron-pyrrole N atoms distance appropriate for low-spin ferric porphyrinates. The Mössbauer data of **1**–**2** feature relatively low values of the quadrupole splitting ($\Delta E_Q \sim 1.20\ mm.s^{-1}$) appropriate for low-spin Fe(III) metalloporphyrin with perpendicular orientation of N-donor planar ligands. The temperature dependence of the magnetic susceptibility and the magnetization curves have shown that the results for complexes **1**–**2** confirm the low-spin state of our two-ferric species, while the cyclic voltammetry data show that the half potential [Fe(III)/Fe(II)] values are shifted anodically compared to the β-pyrrole substituted porphyrin octaethylporphyrin with parallel bis(N-donor) planar axial ligands.

1. Introduction

The main drive for the initial studies on iron metalloporphyrins arose in the elucidation of biological functions of cytochrome P450 enzymes that contain an iron porphyrin unit and are present in most organisms [1]. These biological systems also play an important role in oxygen transfer and as storage agents in hemoglobin and myoglobin and as electron carriers in cytochrome c [2–4]. Additionally, iron(III) porphyrins have attracted much attention as catalysts, i.e., the catalytic C—H insertion using different classes of diazo compounds [5]. A considerable number of important studies devoted to iron(III) metalloporphyrins have established that the axial ligands and the substituted groups at the *meso* and β-pyrrole positions of the porphyrin have direct and important effects on the electronic, magnetic and structural properties of these models [6–8]. It has been reported that iron(III) low-spin hexacoordinated derivatives with N-donor planar axial ligands present two types of configurations of the ground state: (i) the $(d_{xy})^2(d_{xz}, d_{yz})^3$ configuration is usually adopted when the axial ligands present σ-donor character and (ii) the $(d_{xz}, d_{yz})^4(d_{xy})^1$ configuration is shown by either iron(III) porphyrinates with high ruffled porphyrin macrocycle or iron(III) porphyrins carrying weak σ-donating and strong π-accepting ability [9]. The pyridine and the pyrazine species are good σ-donor ligands but the latter have a better π-acceptor character than the pyridine [10]. In the case of low-spin iron(III) six-coordinated metalloporphyrins with the same planar axial ligands (such as substituted imidazoles, pyridines and pyridines), it has been shown that the Mössbauer parameters depends on

* Corresponding author.
E-mail address: habib.nasri@fsm.rnu.tn (H. Nasri).

the relative orientations of the two axial ligands (nearly parallel or nearly perpendicular) [11]. These investigations have highlighted that the porphyrin core deformations, especially the ruffling, minimize the interactions of the *meso*-porphyrin four phenyl rings with the pyridine and substituted pyridines axial ligands [7–12]. Consequently, the planes of the two axial ligands adopt a nearly perpendicular orientation.

On the other hand, the iron(III) low-spin hexacoordinated metalloporphyrins with the non-hindered octaethyporphyrin (OEP) exhibit negligible porphyrin macrocycle deformation. Hence, axial N-donor planar axial ligands are approximately parallel [13].

Notably, from the number of important investigations on iron (III) bis(pyridine) and substituted bis(imidazole) porphyrins reported in the literature [14–17] and in the Cambridge Structural Database [18] only one structure of an iron(III) metalloporphyrin with the related bis(N-donor) planar ligand, namely the pyrazine, is reported with a β-pyrrole substituted porphyrin. This coordination compound is the bis(pyrazine)(2,3,7,8,12,13,17,18-octaethylporphyrinato)iron(III) perchlorate with the formula $[Fe^{III}(OEP)(pyz)_2]ClO_4$ [13]. This species was characterized by NMR ^1H, cyclic voltammetry and single crystal X-ray molecular structure. To gain more insight into the effects of the *meso*-porphyrin and the pyrazine axial ligand on the electronic, magnetic and structural properties of the iron(III) bis(*N*-donor) planar axial ligands metalloporphyrins, we have successfully synthesized two species with the pyrazine as the axial ligand (Scheme 1): the bis(pyrazine)[5,10,15,20-tetra-(*para*-fluorophenyl)porphyrinato]iron(III) triflate (**1**) and the (pyrazine)[5,10,15,20-tetra-(*para*-chlorophenyl)porphyrinato]iron(III) triflate (**2**). These new iron(III) metalloporphyrins were characterized by UV-visible, IR and Mössbauer spectroscopy, magnetic studies, cyclic voltammetry and X-ray molecular structures and are reported here.

2. Experimental section

2.1. Materials and methods

All reagents employed were commercially available and were used as received without further purification. The 5,10,15,20-tetra(*para*-fluorophenyl)porphyrin (H_2TFPP) and the 5,10,15,20-tetra(*para*-chlorophenyl)porphyrin (H_2TClPP) were prepared by using the Alder and Longo method [19] (Scheme SI-1, Supplementary information). All reactions and manipulations for the preparation of the Fe(III) porphyrin derivatives were carried out under aerobic conditions. The chloro iron(III) complexes [Fe(TFPP)Cl] and [Fe(TClPP)Cl] were synthesized as reported in the literature [20] and the triflato iron(III) porphyrin complexes $[Fe^{III}(Porph)(SO_3CF_3)]$ (Porph = TFPP, TClPP) starting materials have been prepared using the literature reported method [21]. Fourier-transformed IR spectra were recorded on a PerkinElmer Spectrum Two FT-IR spectrometer. UV/Vis spectra were recorded with a WinASPECT PLUS (validation for SPECORD PLUS version 4.2). Scanning spectrophotometer mass spectra were recorded with a Bruker autoflex III smartbeam instrument (ESI, positive mode). Cyclic voltammetry (CV) experiments were performed with a CH-660B potentiostat (CH Instruments). All analytical experiments were conducted at room temperature under an argon atmosphere in a standard one-compartment, three-electrode electrochemical cell. Tetra-*n*-butylammoniumhexafluorophosphate ($TBAPF_6$) was used as the supporting electrolyte (0.2 M) in dichloromethane previously distilled over calcium hydride under argon. An automatic Ohmic drop compensation procedure was systematically implemented before the CV data were recorded with electrolytic solutions containing the compounds under study at concentrations of ca. 10^{-3} M. CH Instruments vitreous carbon (Ø = 2 mm) working electrodes were polished with 1 μm diamond paste before each recording. The saturated calomel electrode SCE ($TBAPF_6$ 0.2 M in CH_2Cl_2) redox couple was used as the reference electrode. The potential of the ferrocene/ferrocenium redox couple was used as an internal reference (0.37 V/SCE experimental conditions). All potential are given vs SCE.

Temperature-dependent magnetic susceptibility measurements on polycrystalline samples of **1** and **2** were carried out on a Quantum Design MPMS SQUID susceptometer equipped with a 7 T magnet and operating in the range of temperature from 1.8 to 400 K. The compacted powdered samples were placed in a diamagnetic sample holder and the measurements were carried out in a 1000 Oe applied field using the extraction technique. Magnetization versus magnetic field measurements of **1** and **2** were carried out at 2 K in the field range 0–5 T. The amount of material used for the measurements was 12.86 mg for **1**, 13.31 mg for **2**. Before analysis, the experimental susceptibility was corrected from the sample holder. Diamagnetic corrections of the constituent atoms of **1** and **2** were estimated from Pascal constants [22] with values -295×10^{-6}, -351×10^{-6} $cm^3.mol^{-1}$, respectively.

^{57}Fe Mössbauer spectra were recorded at 78 K with a conventional Mössbauer spectrometer operating in transmission geometry. The samples were sealed in pure aluminum foil and mounted on an Oxford nitrogen bath cryostat. Spectra were fitted to the sum of Lorentzians by a least-squares refinement using Recoil 1.05 Mössbauer Analysis Software [23]. All isomer shifts refer to α-Fe at room temperature.

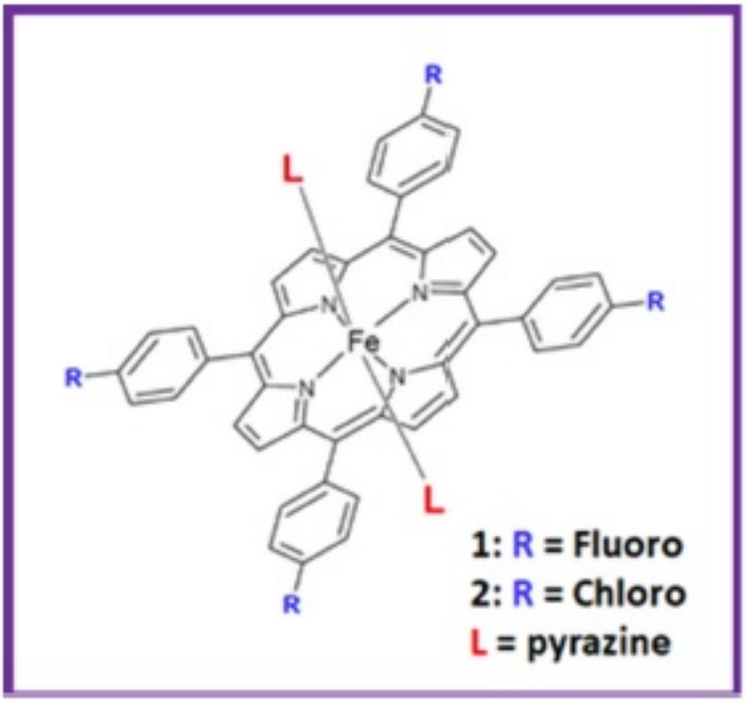

Scheme 1. Schematic representation of complexes 1–2.

2.2. Preparation of complexes 1-2

2.2.1. Synthesis of $[Fe^{III}(TFPP)(pyz)_2](SO_3CF_3)$ (1)

$[Fe^{III}(TFPP)(SO_3CF_3)]$ (50 mg, 0.05 mmol) and pyrazine (80 mg, 1.00 mmol.) were dissolved in dichloromethane (10 mL). The mixture was stirred at room temperature for 4 h. The solution was filtered, and crystals of the complex were prepared by slow diffusion of n-hexane into the dichloromethane solution. Yield 10 mg, 0.01 mmol (20%). $C_{53}H_{32}F_7FeN_8O_3S$ (1049.77): Calcd. C 60.64; H 3.07; N 10.67; Found: C 60.87; H 3.11; N 10.81; UV-visible $[CH_2Cl_2]$: λ_{max} ($\varepsilon \times 10^{-3}$): 417 (2 7 6), 537 (20) nm. IR (KBr disk, cm^{-1}): 3055, 1260, 1081 and 780. MS (ESI+, dichloromethane): m/z = 740.16 $[Fe^{III}(TFPP)]^+$ (Fig. SI-1).

2.2.2. Synthesis of $[Fe^{III}(TClPP)(pyz)_2](SO_3CF_3)$ (2)

Complex **2** was prepared by the procedure given for **1**, except that the TClPP porphyrinato ligand was used instead of TFPP. Good-quality dark purple crystals of **2** were prepared by slow diffusion of n-hexane into the dichloromethane solution. $C_{53}H_{32}Cl_4F_3FeN_8O_3S$ (1115.57): Calcd. C 57.06, H 2.86, N 10.04; found: C, 57.38; H, 2.93; N, 10.11. UV-visible is $[CH_2Cl_2]$: λ_{max} ($\varepsilon \times 10^{-3}$) = 418 (265), 536 (18) nm. IR (KBr disk, cm^{-1}): 3055, 1253, 1030 and 795. MS (ESI+, dichloromethane): m/z = 806.01 $[Fe^{III}(TClPP)+2H]^{3+}$ (Fig. SI-1).

2.3. X-ray structure determination

The data collections for **1** and **2** were performed using a Bruker APEXII CCD Gemini ultra-diffractometer equipped with Mo-Kα radiation source (λ = 0.71073 Å) for **1–2**. Intensity data for all compounds were collected by the narrow frame method. The measurements of the data were done at 298 K for **1** and 200 K for **2**. The reflections were scaled and corrected for absorption effects by using the CrysAlis (R. H. Blessing, (1995)) [24] for **1** and SADABS program (Bruker AXS 2008) [25] for **2**. All structures were solved by direct methods by using SIR-2004 [26] and refined by full-matrix least-squares techniques on F^2 by using the SHELXL-2014 program [27].

3. Results and discussion

3.1. UV-visible and IR spectroscopy

The UV-visible spectra of **1–2** are given as supporting information (Fig. SI-2). It has been reported that the redshift of the Soret and Q absorption bands are related to the nature of the metal center, the electron-withdrawing groups at the *meso* and β-pyrrolic positions and mainly to the non-planar distortion of the porphyrin macrocycle [28–30]. On the other hand, the redshift of the visible absorption bands is responsible for the narrowing of the HOMO–LUMO gap [31]. For the $[Fe^{III}(Porph)(SO_3CF_3)]$ (Porph = TFPP, TClPP) starting materials, the electronic spectra recorded in dichloromethane solutions, the λ_{max} values of the Soret bands at ca. 405 nm while for our two iron(III)-bis(pyrazine) ion complexes (**1–2**), the Soret bands present similar λ_{max} values (at ca. 418 nm) which are quite redshifted compared to those of the iron(III)-triflato starting materials. The redshift of the Soret and Q bands of **1–2** is due to the important porphyrin core deformations of these species (see crystallographic section). We notice that the λ_{max} of the Soret bands of **1–2** are close to those of the related $[Fe^{III}(Porph)(L)_2]^+$ ion complexes where Porph is a *meso*-porphyrinato and L is a monodentate N-donor ligand such as the 2-methyl-imidazole (Table 1).

The IR spectra of our iron(III) derivatives exhibit strong absorption bands at 3055, 3053 cm^{-1} or **1–2**, respectively, which are attributed to the C—H stretching frequency of the pyrazine axial ligand. For each bis(pyrazine) ion complex, three absorption bands are observed: at 1260, 1081 and 780 cm^{-1} (for **1**), 1253, 1030 and 795 cm^{-1} (for **2**) which are attributed to the triflate $SO_3CF_3^-$ counterion [21].

3.2. X-ray structures of 1–2

Complexes **1–2** crystallize in the monoclinic crystal system with the same space group C2/c. Indeed, **1–2** are isostructures as shown by the very similar cell parameters values and many other structural properties discussed later in this section. The crystallographic data and selected bond lengths [Å] and angles [°] for **1–2** are given in Table SI-1 and Table SI-2 (Supplementary information), respectively. The asymmetric units of **1–2** are made by one $[Fe^{III}(Porph)(pyz)_2]^+$ (Porph = TFPP, TClPP) ion complex and one triflate $(SO_3CF_3)^-$ counterion. The ortep diagrams of the $[Fe^{III}(Porph)(pyz)_2]^+$ ion complexes (Porph = TFPP for **1** and TClPP for **2**) are illustrated in Fig. 1. The $[Fe^{III}(Porph)(pyz)_2]^+$ ions complexes (**1** and **2**) exhibit a distorted octahedron coordination geometry where the equatorial plane is formed by the four nitrogen atoms of the porphyrin and the apical positions are occupied by two pyrazine ligands.

The two distances between the iron and the nitrogen atom of the pyrazine axial ligands are 1.994(2) Å/2.005(2) Å and 1.994(2) Å/2.007(2) Å for **1** and **2** respectively, which are close to those of the related OEP $[Fe^{III}(OEP)(pyz)_2]^+$ derivative and the bis(pyridine) ion complex $[Fe^{III}(TPP)(pyz)_2]^+$ (Table 2).

The porphyrin macrocycles of **1–2** showing the displacements of each atom from the mean plane of the 24-atom porphyrin core in units of 0.01 Å are represented in Fig. 2. Classically, the porphyrin macrocycle can be characterized by four major deformations [32], **namely**: (1) the *ruffling* distortion (*ruff*) is indicated by the values of the meso-carbon atoms above and below the porphyrin mean plane, (2) the *doming* distortion (*dom*) is often observed in five-coordinated porphyrin complexes when the axial ligand causes a displacement of the metal center out of the mean plane, and the nitrogen atoms are also displaced toward the axial ligand, (3) *the saddle* distortion (*sad*) involves the displacement of the pyrrole rings alternately above and below the mean porphyrin macrocycle so that the pyrrole nitrogen atoms are out of the mean plane, (4) in the *waving* distortion (*wav*), the four fragments «(β-carbon)-(α-carbon)-(*meso*-carbon)-(α-carbon)-(β-carbon)» (or Cβ-Cα-Cm-Cα'-Cβ') are alternatively above and below the 24-atoms of the $C_{20}N_4$ least squares plane of the porphyrin core. As illustrated by Fig. SI-3 and Fig. 2, complexes **1** and **2** present important *ruffling* and *waving* distortions.

Scheidt and Reed [33] have shown that the value of the average equatorial iron-pyrrole N atoms distance (Fe—Np) and the spin-state of the iron(III) metalloporphyrins are related. Thus, for six-coordinated Fe(III) high-spin (HS) (S = 5/2) porphyrins, the values of Fe—Np are usually higher than 2.037 Å while for iron(III) low-spin (LS) (S = 1/2) metalloporphyrins, the Fe—Np values are smaller than those of the HS species and range between 1.998 Å and 1.952 Å

Table 1
UV-visible data of our synthetic *meso*-porphyrins and selected iron(III) metalloporphyrins.

Complex	Soret band λ_{max} [nm] ($\varepsilon \times 10^{-3}$ ($Lmol^{-1}.cm^{-1}$))	Q bands λ_{max} [nm] ($\varepsilon \times 10^{-3}$ ($Lmol^{-1}.cm^{-1}$))	References
H_2TFPP	419 (337)	516 (21), 552 (13), 594 (6), 651 (3)	This work
H_2TClPP	420 (340)	515 (23), 548 (11), 593 (7), 646 (4)	This work
$[Fe^{III}(TFPP)(SO_3CF_3)]$	404 (105)	516 (10)	This work
$[Fe^{III}(TClPP)(SO_3CF_3)]$	406 (106)	515 (11)	This work
$[Fe^{III}(TFPP)(pyz)_2]^+$ (1)	417 (276)	537 (20)	This work
$[Fe^{III}(TClPP)(pyz)_2]^+$ (2)	418 (265)	536 (18)	This work
$[Fe^{III}(TMPP)(2\text{-}Melm)_2]$	417	560, 582	[11]
$[Fe^{III}(TMPP)(1\text{-}Melm)_2]$	416	550, 580	[11]

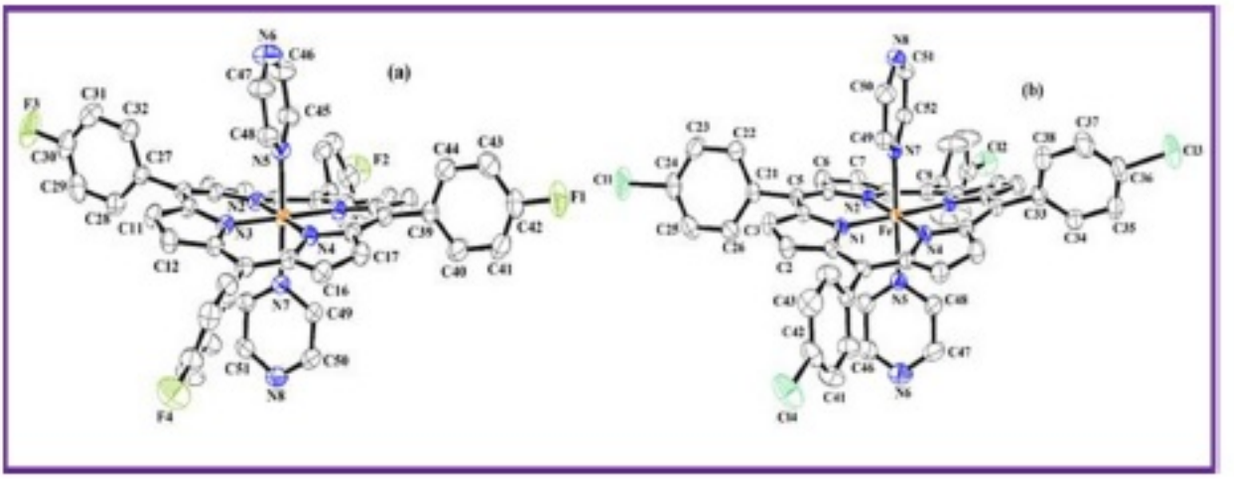

Fig. 1. ORTEP diagrams of the $[Fe^{III}(TFPP)(pyz)_2]^+$ ion complex: (a), $[Fe^{III}(TClPP)(pyz)_2]^+$ ion complex: (b). Ellipsoids are drawn at 40%. The hydrogen atoms are omitted for clarity.

Table 2
Selected structural features of several six-coordinated iron(III) metalloporphyrins.

Complex	Fe –Np[a] (Å)	Fe – Lax[b] (Å)	Spin S	ϕ[c] (in °)	References
$[Fe^{III}(TPP)(H_2O)_2]^+$	2.045	2.095	5/2	–	[35]
$[Fe^{III}(OEP)(NCS)(py)]$[d]	2.048	2.031/2.442	5/2	–	[36]
$[Fe^{III}(TPP)(NCS)(py)]$[e]	2.06	1.97/2.40	5/2	–	[37]
$Fe^{III}(TPP)(F)_2]^+$	2.064	1.966	5/2	–	[38]
$[Fe^{III}(OEP)(DMSO)_2]^+$[f]	2.037	2.083	5/2	–	[39]
$[Fe^{III}(TPP)(4\text{-}MeHlm)_2]^+$[g]	1.9980	1.928/1.958	1/2	–	[14]
$[Fe^{III}(TPP)(Hlm)_2]^+$[h]	1.993	1.964	1/2	–	[15]
$[Fe^{III}(TPP)(2\text{-}MeHlm)_2]^+$[j]	1.970	2.012	1/2	–	[40]
$[Fe^{III}(TPP)(N_3)(py)]$[k]	1.989(6)	2.089/1.925	1/2	–	[41]
$[Fe^{III}(TPP)(py)_2]^+$	1.982	2.005/2.001	1/2	–	[16]
$[Fe^{III}(TPP)(4\text{-}CNPy)_2]^+$[l]	1.952(7)	2.002(8)	1/2	–	[12]
$[Fe^{III}(OEP)(3\text{-}ClPy)_2]^+$[m]	1.994(2)	2.031(2)	1/2	0.0	[17]
$[Fe^{III}(OEP)(pyz)_2]^+$	1.985(15)	2.005(16)	1/2	0.0	[13]
$[Fe^{III}(TFPP)(pyz)_2]^+$(1)	1.9693(18)	1.994(2)/2.005(2)	1/2	86.87(7)	This work
$[Fe^{III}(TClPP)(pyz)_2]^+$ (2)	1.9668(16)	1.994(2)/2.007(2)	1/2	88.58(7)	This work

[a] Fe–Np = average equatorial distance between the iron and the nitrogen atoms of the porphyrin ring.
[b] Fe–Lax = iron-axial ligand distance.
[c] ϕ = dihedral angle between the two axial ligands (relative orientation).
[d] OEP = octaethylporphyrinato.
[e] TPP = meso-tetraphenylporphyrinato.
[f] DMSO = dimethylsulfoxide.
[g] 4-MeHlm = 4-methylimidazole.
[h] Hlm = imidazole.
[j] 2-MeHlm = 2-methylimidazole.
[k] N_3^- = azido.
[l] 4-CNpy = 4-cyanopyridine.
[m] 3-Clpy = 3-chloropyridine.

(Table 2). In our case, complexes **1** and **2** exhibit Fe—Np bond length values of 1.9693(18) Å and 1.9668(16) Å, respectively, indicating that these iron(III) derivatives are unambiguously LS. It has been shown that for iron(III) metalloporphyrins, the Fe—Np bond length value is related to the deformation of the porphyrin core; the Fe—Np distance decreases as the porphyrin ring is more distorted [7,11]. Thus, in the case of the related iron(III) bis(pyrazine) derivative with the octaethyporphyrinate (OEP) which is known to be present in a very planar porphyrin core because of the absence of steric effects, the Fe—Np bond length is 1.985 (2) Å [13]. The shortened Fe—Np bond leads to both strong σ and π interactions between the iron(III) and the porphyrin [7]. Therefore, the short Fe—Np distances of our TFPP and TClPP derivatives compared to the related OEP-bis(pyrzine) species are due to the significant deformation of the porphyrin macrocycles of these two *para*-halogeno substituted *meso*-phenylporphyrins. It is noteworthy that for the sterically "hindered" porphyrin and substituted pyridines axial ligands, due to the strong *ruffling* of the porphyrin ring, two "ligand binding pockets" are formed where these asymmetric ligand binding cavities have approximately perpendicular orientations which are thought to be responsible for the relative perpendicular orientations of the planes of the two axial ligands [11]. Consequently, the greater the deformation of the porphyrin core, the closer to 90° is the dihedral angle ϕ between the two planes of the pyz ligands. Explicitly, this angle is that between the two "N5-C45-C46-N6-C47-C48" and "N7-C49-C50-N8-C51-C52" moieties for complexes **1–2**. In Fig. SI-4 (Supplementary information) depicts the two "ligand binding pockets" of complexes **1–2** which are nearly perpendicular. For **1–2**, the ϕ dihedral angle values are 86.87(7)° for **1** and 88.58(7)° for **2**. Notably, for the related bis(pyrazine) iron(III) complex with the non-hindered octaethyporphyrin (OEP), with the formula $[Fe^{III}(OEP)(pyz)_2]ClO_4$, [13], the dihedral ϕ angle value is zero due to symmetric consideration because the iron central metal occupies an inversion center. The porphyrin place of this iron(III)-OEP derivative is practically planar which explain the parallel orientation of the pyz axial ligands.

As will be discussed in the Mössbauer section, the perpendicular orientations of the axial ligands have an implication on the

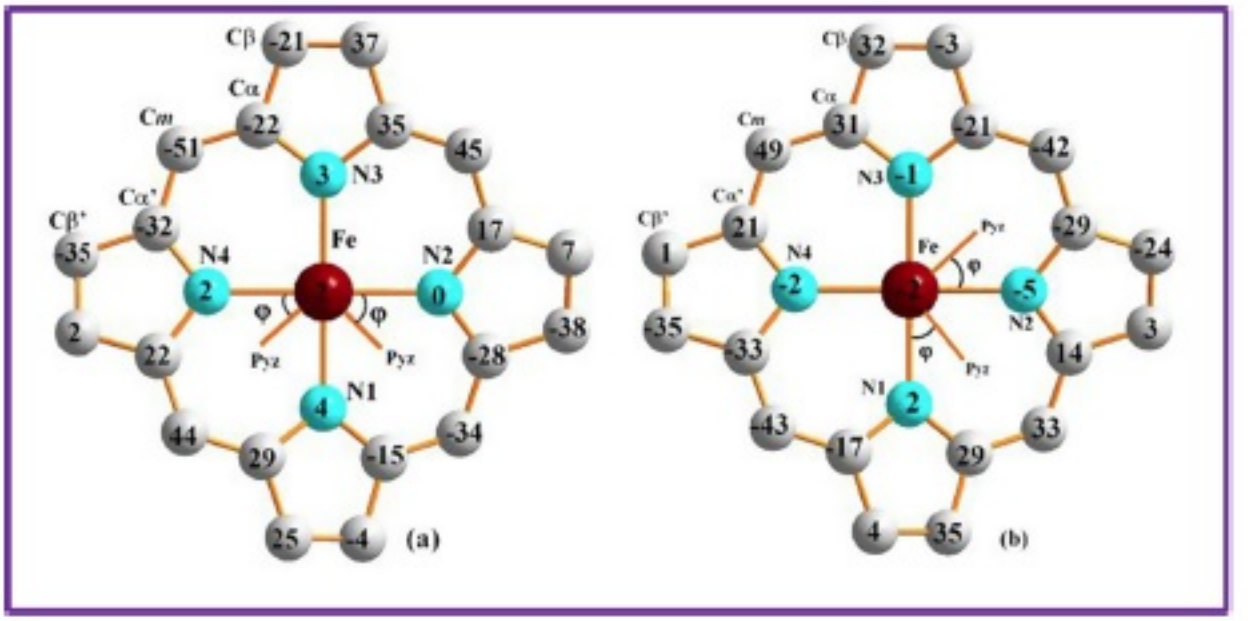

Fig. 2. Formal diagrams of the porphyrinato cores of 1–2. (a): complex 1 and (b): complex 2. The displacements of each atom from the 24-atom core planes in units of 0.01 Å are also illustrated. The diagrams show also the φ angle between the axial pyz ligands and the closest N(pyrrole)-Fe-N(pyz) plane.

Mössbauer parameters of the iron(III) low-spin metalloporphyrins. In this case, the values of the dihedral angle (φ) between the pyrazine plane and the closest N(pyrrole)-Fe-N(pyz) plane (for the first and second pyz axial ligands) are 42.92°/44.28° and 42.97°/41.43° for **1–2**, respectively. These values are quite close to the value 45° which leads to a minimum nonbonded interaction between the porphyrin core atoms and the planar axial ligand hydrogen atoms [34,11]. Consequently, the two pyrazine planes are close to eclipsing adjacent Fe-C(*meso*) vectors. However, the pyrazine axial ligands are offset from the two *trans* N pyrrole atoms. Thus, the values of the closest angle between the pyz axial ligand and the vector made by two *trans* N pyrrole atoms and the iron(III) ion, are 52.80°/45.48° and 47.01°/43.08° for **1–2**, respectively.

In the crystal of the iron(III) bis(pyrazine)-TFPP compound (**1**), two adjacent $[Fe^{III}(TFPP)(pyz)_2]^+$ ions complexes are linked to each other by two C—H···O interactions between a carbon atom of one pyz axial ligand and an oxygen atom of the $SO_3CF_3^-$ counterion (Fig. SI-5, Table SI-3). The crystal packing of **1** is further sustained by weak C—H···F non-conventional hydrogen bond between a carbon of a phenyl group of one porphyrin and a fluorine atom of an adjacent porphyrin with a distance of 3.075(3) Å (Fig. SI-6). Crystal structure of the iron(III) bis(pyrazine)-TClPP species (**2**) features weak Cg···Cg aromatic π interactions between the centroids of two pyz rings of two neighboring porphyrins (Fig. SI-7, Table-SI-4) with a Cg···Cg distance value of 3.5530(12) Å.

3.3. Mössbauer spectroscopy

^{57}Fe Mössbauer spectra of microcrystalline samples of **1–2** were recorded at 78 K (Fig. 3). We consider an orientation of the two planar axial ligands as parallel when the dihedral angle ϕ (relative orientation) is between 0 and 40°, while for a perpendicular orientation of the two axial ligands the ϕ angle is between 80 and 90°. Safo et al. [11] indicated that for six-coordinated LS iron (III) porphyrins with two planar axial ligands such as substituted-imidazoles or substituted-pyridines, the values of the isomeric shift (δ) and the quadrupole splitting (ΔE_Q) are related to the relative orientation of the two planes of the axial ligands. Thus, for a parallel orientation of the axial ligands, the δ and ΔE_Q values are ~0.25 mm.s^{-1} and ~2.25 mm.s^{-1}, respectively. For a perpendicular orientation, the values of δ and ΔE_Q are smaller than those observed for a parallel orientation with a typical values of δ ~ 0.20 mm.s^{-1} and ΔE_Q values between 1.75 and 0.90 mm.s^{-1} (Table 3).

The spectra of **1–2** are fitted considering one unique doublet with very close isomer shift and quadrupole splitting values (δ/ΔE_Q in mm.s^{-1}) of 0.21(5)/1.15(1) for **1** and 0.22(6)/1.22(1) for **2**. These Mössbauer parameters are characteristic of low-spin (S = 1/2) Fe(III) metalloporphyrins with perpendicular axial ligand orientation which is confirmed by the molecular structures of these species (see crystallographic section).

We notice that the δ and ΔE_Q values of our two bis(pyrazine) porphyrinates are very close to those of the low-spin iron(III) bis(pyridine) derivative with the *meso*-tetraphenylporphyrin coordination compound $[Fe^{III}(TPP)(py)_2]^+$ which indicate that (i) the electronic and steric effect of the pyridine and the pyrazine are practically the same (ii) the fluoro and the chloro *para*-substituting on the phenyl rings of the TPP porphyrinato ligand have no effect on the Mössbauer parameters. Unfortunately, we cannot compare our Mössbauer data with those of the iron(III).bis(pyrazine) octaethylporphyrin complex which is not available in the literature (even though the molecular structure and the CV data are published). Nevertheless, for the bis{4-(dimethylamino)pyridine} ion complex with the OEP porphyrin $[Fe^{III}(OEP)(4\text{-}NMe_2py)_2]^+$, the δ and ΔE_Q values are different from those of our bis(pyrazine) species with a values of 0.26 mm.s^{-1} and 2.14 mm.s^{-1} which are characteristic of low-spin iron(III) bis(N-donor) planar axial ligands with parallel orientation.

3.4. Magnetic susceptibility measurements

Magnetic properties were investigated for the two iron(III)-bis(pyz) porphyrin derivatives via SQUID magnetometry over the temperature range 2–300 K. The $\chi_M T$ curves (χ_M is the magnetic susceptibility) versus the temperature of our two iron(III) derivatives are shown in Fig. SI-8 while plots of the effective magnetic moment (μ_{eff}) versus the temperature of the polycrystalline samples of **1–2** are illustrated in Fig. 4. The plots of **1–2** are very similar with a very small variation of the μ_{eff} values from low temperature to room temperature. Thus, for **1–2**, at 2.0 K, the μ_{eff} values are 1.73 μ_B and 1.68 μ_B, respectively, while at 300 K these values are 2.09 μ_B and 2.0 μ_B. These results are appropriate for low-spin (S = 1/2) iron(III) compounds with g = 2 and a significant orbital contribution. Increasing the temperature results in a gradual increase

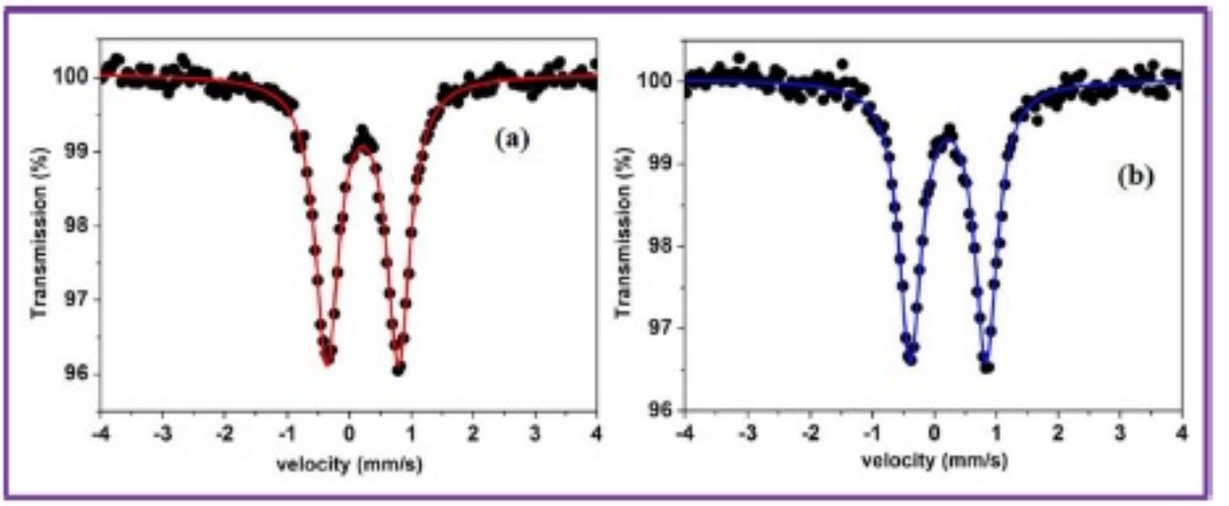

Fig. 3. Solid Mössbauer spectra taken at 78 K of complex 1 (a) and complex 2 (b).

Table 3
List of hyperfine parameters deduced by microcrystalline 57Fe Mössbauer spectroscopy for several low-spin Fe(III) porphyrin complexes with planar bis(*N*-donor) axial ligands.

Compound	Parameters					References
	T (K)	δ (mm/s)	ΔE_Q (mm/s)	ϕ[a] (in °)	Γ/2 (mm.s^{-1})[b]	
$[Fe^{III}(TFPP)(pyz)_2]SO_3CF_3$ (1)	78	0.21(5)	1.15(1)	86.87(7)	0.21(1)	This work
$[Fe^{III}(TClPP)(pyz)_2]SO_3CF_3$ (2)	78	0.22(6)	1.22(1)	88.58(7)	0.21(1)	This work
$[Fe^{III}(TMP)(3\text{-Etpy})_2]ClO_4$[c,d]	77	0.18	1.25	86	–	[42]
$[Fe^{III}(TPP)(py)_2]ClO_4$[e]	77	0.16	1.25	86	–	[16]
$[Fe^{III}(TMP)(3\text{-Clpy})_2]ClO_4$[f]	77	0.20	1.36	88	–	[7]
$[Fe^{III}(TMP)(2\text{-MeHlm})]ClO_4$[g]	77	0.20	1.48	88	–	[7]
$[Fe^{III}(TMP)(4\text{-CNpy})]ClO_4$[h]	77	0.20	0.97	87	–	[7]
$[Fe^{III}(OEP)(4\text{-NMe}_2py)_2]ClO$[k,l]	77	0.26	2.14	0	0.22	[11]
$[Fe^{III}(OMTPP)(1\text{-MeHlm})_2]Cl$[m,n]	77	0.28	2.78	19.5	–	[43]
$[Fe^{III}(TMP)(4\text{-NMe}_2py)_2]ClO_4$	77	0.20	1.74	90	–	[11]

[a] ϕ = Dihedral angle between the two axial ligands (relative orientation).
[b] Γ/2 = half linewidth at half maximum.
[c] TMP = meso-tetramesitylporhyrinato.
[d] 3-Etpy = 3-ethylpyridine.
[e] TPP = meso-tetraphenylporphyrinato.
[f] 3-Clpy = 3-chloropyridine.
[g] 2-MeHlm = 2-methylimidazole.
[h] 4-CNpy = 4-cyanopyridine.
[k] OEP = octaethylporphyrinato.
[l] 4-NMe2py = 4-(dimethylamino)pyridine.
[m] OMTPP = octaalkyltetraphenylporphinato.
[n] 1-MeHlm = 1-methylimidazole.

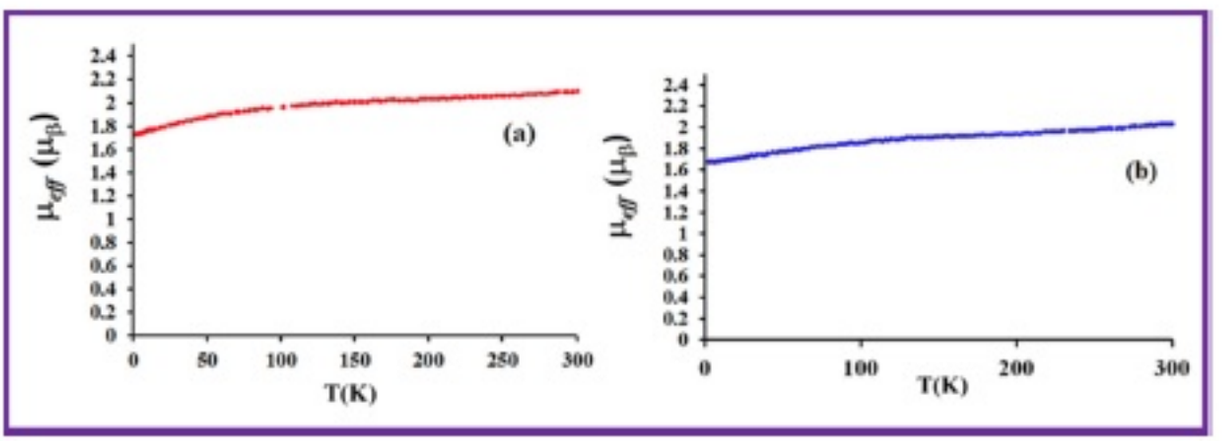

Fig. 4. Temperature dependence of the effective magnetic moment (μ_{eff}). (a): $[Fe^{III}(TFPP)(pyz)_2](SO_3CF_3)$ (1). (b): $[Fe^{III}(TClPP)(pyz)_2](SO_3CF_3)$ (2).

in the magnetic moment indicating that the orbital contribution is not negligible. This is characteristic of a low-spin octahedral iron (III) systems with spin-orbit coupling of the $^2T_{2g}$ ground term, as already reported in the literature [44]. The field dependence of the magnetization, M = f(H), at 2 K is given in Fig. SI-9. The experimental M values are compatible with the theoretical ones calculated using the Brillouin function with S = 1/2 ground state and g = 2 for complexes **1–2**.

3.5. Cyclic voltammetry

The electrochemical behavior of **1–2** was studied by cyclic voltammetry (CV) with tetra-n-butylammonium hexafluorophosphate ($TBAPF_6$) as the supporting electrolyte (0.2 M) in the non-coordinating solvent dichloromethane under an argon atmosphere. The CV of these species are illustrated in Fig. 5 and the values of half potential waves of our two derivatives along with other related iron(III) metalloporphyrins are given in Table 4. The CV data of complexes **1–2** are practically the same. Indeed, the anodic part of the cyclic voltammogram of **1–2** includes one electron reversible oxidation wave of the iron [Fe(III)/Fe(IV)] with $E_{1/2}$ value of ~1.20 V. The second one-electron reversible oxidation wave of **1–2** complexes are attributed to the oxidation of the porphyrin ring where the $E_{1/2}$ value is ~1.40 V. The cathodic part of the cyclic voltammograms of **1–2** exhibit one-electron reversible reduction wave of the Fe(III) with a half-potential value $E_{1/2}$ ([Fe(III)/Fe(II)) of ~0.30 V. The one-electron quasi-reversible reduction wave at $E_{1/2} \sim -1.70$ V could be attributed to the porphyrin ring reduction. The Fe(III)/Fe(II) reduction of iron(III) metalloporphyrins has been best studied by cyclic voltammetry and several attempts have been made to correlate the changes of the $E_{1/2}$ [Fe(III)/Fe(II)] value with metal spin state, axial-ligand coordination, basicity of the porphyrin ring, counterion and the deformation of the porphyrin core [45]. We notice that the hexacoordinated low-spin iron(III) *meso*-porphyrinates with bis(N-bond) nitrogen planar axial ligands type $[Fe^{III}(Porph)(L)_2]^+$, with a perpendicular orientations of these ligands, exhibit Fe(III)/Fe(II) half potential values shifted toward more positive potential values compared to the β-substituted porphyrin OEP (octaethylporphyrin) with parallel bis(N-donor) planar ligands [13]. For example, the $E_{1/2}$ [Fe(III)/Fe(II)] value is 0.16 V for the bis(pyridine) ion complex $[Fe^{III}(TPP)(py)_2]^+$ [46] and −0.16 V

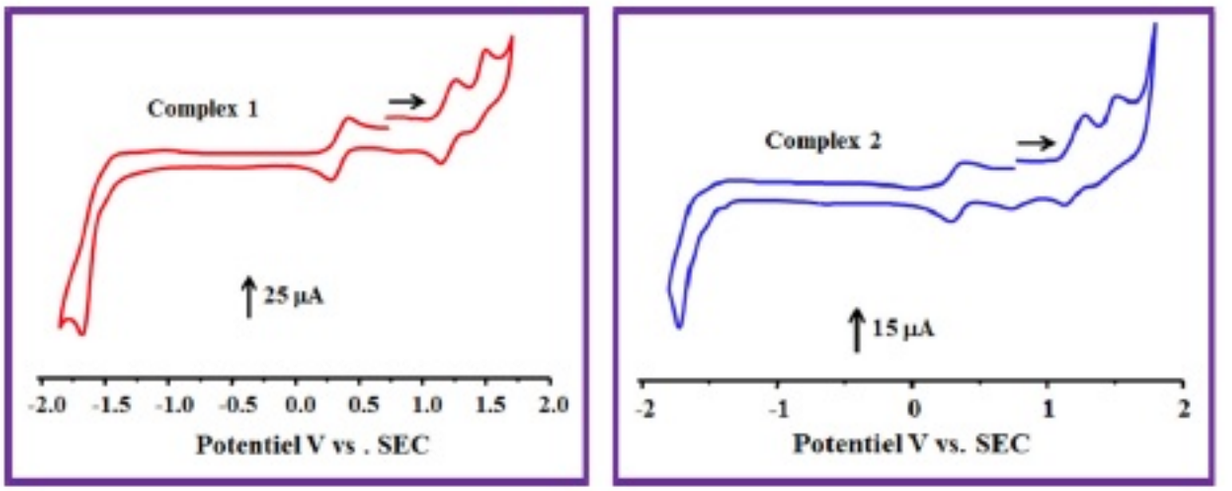

Fig. 5. Cyclic voltammograms of complexes 1 and 2. The solvent is CH_2Cl_2 and the concentration is ca. 10–3 M in 0.2 M TBAPF6, 100 mV/s, vitreous carbon working electrode (Ø = 2 mm).

Table 4
Electrochemical data[a] for 1–2 and a selection of related low-spin iron(III) metalloporphyrins in CH_2Cl_2 (exceptions are indicated).

Complex	Oxidations				Reductions				References
	Ring oxid	Fe(III)/Fe(IV)			Fe(III)/Fe(II)			Ring reduc.	
	$E_{1/2}$[b]	E_{pa}[c]	E_{pc}[d]	$E_{1/2}$	E_{pa}	E_{pc}	$E_{1/2}$	$E_{1/2}$	
$[Fe^{III}(TPP)(4\text{-}CNpy)_2]^+$[e,f,g]	–	–	–	–	–	–	0.16	–	[46]
$[Fe^{III}(TPP)(3,4\text{-}Me_2Py)_2]^+$[h]	–	–	–	–	–	–	0.138	–	[46]
$[Fe^{III}(TPP)(NMeIm)_2]^+$[i]	–	–	–	–	–	–	−0.089	–	[46]
$[Fe^{III}(TPP(2\text{-}6Cl))(4\text{-}CNpy)_2]^+$[j]	–	–	–		–	–	0.34	–	[46]
$[Fe^{III}(OEP)(pyz)_2)]^+$[k]	1.59	–	–	1.23	–	–	−0.20	–	[17]
$[Fe^{III}(OEP)(py)_2)]^+$[l]	–	–	–	–	–		−0.16	–	[47]
$[Fe^{III}(OEP)(1\text{-}NMeIm)_2)]^+$[m]	–	–	–	–	–	–	−0.39	–	[47]
$[Fe^{III}(OEP)(4\text{-}NH_2Py)_2)]^+$[n]	–	–	–	–	–	–	−0.39	–	[47]
$[Fe^{III}(TPP)(2\text{-}6F)(py)_2]^+$[o]	–	–	–	–	–	–	0.35	–	[46]
$[Fe^{III}(TPP)(py)_2]^+$	–	–	–	–	–	–	0.16	–	[46]
$[Fe^{III}(TFPP)(pyz)_2)]^+$ (1)	1.43	1.25	1.14	1.19	0.37	0.27	0.32	−1.73	This work
$[Fe^{III}(TClPP)(pyz)_2]^+$ (2)	1.44	1.27	1.13	1.20	0.38	0.28	0.33	−1.72	This work

[a] The potentials are reported versus SCE.
[b] $E_{1/2}$ = half-wave potential.
[c] E_{pa} = anodic peak potential.
[d] E_{pc} = cathodic peak potential.
[e] TPP = *meso*-tetraphenylporphyrinato.
[f] DMF = in *N,N*-dimethylformamide solvent.
[g] CNpy = 4-cyanopyridine.
[h] 3,4-Me2Py = 3,4-(dimethylpyridine).
[i] *N*-MeHIm = *N*-methylimidazole.
[j] TPP(2-6Cl) = 5,10,15,20-tetrakis(2,6-dichlorophenyl)porphyrinato.
[k] OEP = octaethylporphyrinato.
[l] py = pyridine.
[m] 1-MeHIm = 1-methylimidazole.
[n] 4-NH2Py = 4-aminopyridine.
[o] TPP(2-6F) = 5,10,15,20-tetrakis(2,6-difluorophenyl)porphyrinato.

for the $[Fe^{III}(OEP)(py)_2]^+$ species [47]. It is noteworthy that the $[Fe^{III}(TPP)(2,6F)(py)_2]^+$ and the $[Fe^{III}(TPP)(2,6Cl)(4\text{-}CNpy)_2]^+$ ions complexes where (TPP)(2,6F) and (TPP)(2,6Cl) are the *ortho*, *para*-fluoro and the *ortho*, *para*-chloro substituted phenyl ring of the *meso*-tertaphenylporphyrin feature $E_{1/2}$ [Fe(III)/Fe(II)] values shifted anodically relative to the non-substituted tetraphenylporphyrin derivative type $[Fe^{III}(TPP)(L)_2]^+$ where L is a bis(N-donor) planar axial ligands (Table 4). The $E_{1/2}$ [Fe(III)/Fe(II)] values or our species (**1–2**) which are observed in the positive-potential region [$E_{1/2}$ at ca. 0.30 V] confirm what we mentioned above. Thus, these values are different from the OEP related species $[Fe^{III}(OEP)(pyz)_2]^+$ ($E_{1/2}$ = −0.20 V) with parallel orientation of the pyrazine planes. These half potential values are close to those of the halogeno substituted phenyl rings *meso*-porphyrin iron(III) derivatives type $[Fe^{III}(Porph)(L)_2]^+$ (L = planar *N*-donor axial ligand) (Table 4). The CV investigation confirms that our iron(III)-bis(pyrazine) TFPP and the TClPP derivatives exhibit very close electronic and electrochemical properties and that the iron(III) complexes with bis(pyrazine) and bis(pyridine) have very close electronic and steric properties.

4. Conclusion

In Summary, the iron(III) bis(pyrazine) derivatives with the fluoro and chloro *para*-substituted *meso*-tetraphenylporpyrin (TFPP and TClPP) exhibit very close UV-visible, Mössbauer, structural, magnetic and electrochemical properties characteristic of iron(III) low-spin (S = 1/2) hexacoordinated *meso*-porphyrin complexes with nearly perpendicular pyrazine axial ligands. Our two bis(pyrazine) iron(III) species show very similar properties to each other than the bis(pyridine) and bis(substituted pyridines) iron(III) *meso*-porphyrin metalloporphyrines. Nevertheless, the structural, electronic and magnetic properties of the related hexacoordinated complex with the β-pyrrole substituted octaethylporphyrin (OEP) with the formula $[Fe^{III}(OEP)(pyz)_2]^+$ are very different with those of our two synthetic models $[Fe^{III}(TFPP)(pyz)_2]^+$ and $[Fe^{III}(TClPP)(pyz)_2]^+$ ion complexes.

Acknowledgement

The authors gratefully acknowledge financial support from the Ministry of Higher Education and Scientific Research of Tunisia.

Appendix A. Supplementary data

Supplementary data associated with this article can be found, in the online version, at https://doi.org/10.1016/j.ica.2018.02.016.

References

[1] Y. Deng, J.M. Huang, Chem. Phys. 321 (2006) 133.
[2] P.J. Collman, C. Paul, C.P. Herrmann, L. Fu, A. Todd, T.A. Eberspacher, E.M. Michael, B. Boitrel, P. Hayoz, X.L. Zhang, J.J. Brauman, V.W. Day, J. Am. Chem. Soc. 119 (1997) 3481.
[3] M.R. Preimesberger, A. Majumdar, J.T.J. Lecomte, Biochemistry (2017) 2.
[4] J. Yi, L.M. Thomas, F.N. Musayev, M.K. Safo, G.R. Addo, Biochemistry 50 (2011) 8323.
[5] M.H. Mbuvi, L.K. Woo, Organometallics 27 (2008) 637.
[6] R.J. Cheng, P.Y. Chen, P.R. Gau, C.C. Chen, S.M. Peng, J. Am. Chem. Soc. 119 (1997) 2563.
[7] M.K. Safo, G.P. Gupta, C.T. Watson, U. Simonis, F.A. Walker, W.R. Scheidt, J. Am. Chem. Soc. 114 (1992) 7066.
[8] R. Weiss, J. Fischer, V. Bulach, J.A. Shelnutt, C. R. Chimie 5 (2002) 405.
[9] M. Nakamura, Y. Ohgo, A. Ikezaki, J. Inorg. Biochem. 102 (2008) 433.
[10] J.S. Haynes, J.R. Sams, R.C. Thompson, Inorg. Chem. 25 (1986) 3740.
[11] M.K. Safo, G.P. Gupta, F.A. Walker, W.R. Scheidt, J. Am. Chem. Soc. 113 (1991) 5497.
[12] M.K. Safo, F.A. Walker, A.M. Raitsimring, W.P. Walters, D.P. Dolata, P.G. Debrunner, W.R. Scheidt, J. Am, Chem. Soc. 116 (1994) 7760.
[13] M.K. Motlagh, M. Noroozifar, J. Saffari, A. Naeimi, B.O. Patrick, Inorg. Chim. Acta 362 (2009) 2861.
[14] R. Quinn, C.E. Strouse, J.S. Valentine, Inorg. Chem. 22 (1983) 3934.
[15] W.R. Scheidt, S.R. Osvath, Y.J. Lee, J. Am. Chem. Soc. 109 (1987) 1958.
[16] D. Inniss, S.M. Soltis, C.E. Strouse, J. Am. Chem. Soc. 110 (1988) 5644.
[17] W.R. Scheidt, D.K. Geiger, K.J. Haller, J. Am. Chem. Soc. 104 (1982) 495.
[18] F.H. Allen, Acta Cryst. B58 (2002) 380.
[19] A.D. Adler, F.R. Longo, J.D. Finarelli, J. Goldmacher, J. Assour, L.A. Korsakoff, J. Org. Chem. 32 (1967) 476.
[20] J.P. Collman, R.R. Gagne, C. Reed, T.R. Halbert, G. Lang, W.T. Robinson, J. Am. Chem. Soc. 97 (1975) 1427.
[21] A. Gismelseed, E.L. Bominaar, E. Bill, A.X. Trautwein, H. Winkler, H. Nasri, P. Doppelt, D. Mandon, J. Fischer, R. Weiss, Inorg. Chem. 92 (1990) 2741.
[22] A. Earnshaw, Introduction to Magnetochemistry, first ed., Academic Press, New York, London, 1968, pp. 1–4.
[23] K. Lagarec, D.G. Rancourt, Recoil, Mössbauer Spectral Analysis Software for Windows [1.0], Department of Physics, University of Ottawa, Canada, 1998.
[24] R.H. Blessing, Acta. Cryst. A 51 (1995) 33.
[25] SMART, SAINT, and SADABS, Bruker AXS Inc., Madison, WI, (2008).
[26] A. Altomare, G. Casacarano, C. Giacovazzo, A. Guagliardi, M.C. Burla, G. Polidori, M.J. Camalli, Appl. Crystallogr. 27 (1994) 435.
[27] G.M. Sheldrick, Acta Crystallogr. C71 (2015) 3.
[28] L. Jiang, R.A. Zaenglein, J.T. Engle, C.M. Mittal, C.S. Hartley, C.J. Ziegler, H. Wang, J. Chem. Commun. 48 (2012) 6927.
[29] R. Weiss, J. Fischer, V. Bulach, V. Schünemann, M. Gerdan, A.X. Trautwein, J.A. Shelnutt, C.P. Gros, A. Tabard, R. Guilard, Inorg. Chem. Acta 337 (2002) 223.
[30] J.A. Shelnutt, The Porphyrin Handbook, eds K. M. Kadish, K. M. Smith, R. Guilard, Academic Press, San Diego, 167, 2000.
[31] K.M. Barkigia, L. Chantranupong, K.M. Smith, J. Fajer, J. Am. Chem. Soc. 110 (1988) 7566.
[32] W.R. Scheidt, Y. Lee, Struct. Bond. (Berlin) 64 (1987) 1.
[33] W.R. Scheidt, C.A. Reed, Chem. Rev. 81 (1981) 543.
[34] W.R. Scheidt, D.K. Geiger, R.G. Hayes, G. Lang, J. Am. Chem. Soc. 105 (1983) 2625.
[35] M.E. Kastner, W.R. Scheidt, T. Mashiko, C.A. Reed, J. Am. Chem. Soc 100 (1978) 666.
[36] W.R. Scheidt, Y.J. Lee, D.K. Geiger, K. Taylor, K. Hatano, J. Am. Chem. Soc. 104 (1982) 3367.
[37] D.K. Geiger, V. Chunplang, W.R. Scheidt, Inorg. Chem. 24 (1985) 4736.
[38] W.R. Scheidt, Y.J. Lee, J. Am. Chem. Soc. 105 (1983) 778.
[39] M. Mylrajan, L.A. Andersson, J. Sun, T.M. Loehr, C.A. Thomas, E.P. Sullivan, M.A. Thomson, K.M. Long, O.P. Anderson, Inorg. Chem. 34 (1995) 3953.
[40] W.R. Scheidt, J.F. Kirner, J.L. Hoard, C.A. Reed, J. Am. Chem. Soc. 109 (1987) 1963.
[41] K.M. Adams, P.G. Rasmussen, W.R. Scheidt, Inorg. Chem. 18 (1979) 1892.
[42] D.A. Summerville, I.A. Cohen, K. Hatano, W.R. Scheidt, Inorg. Chem. 17 (1978) 2906.
[43] T. Teschner, L. Yatsunyk, V. Schünemann, H. Paulsen, H. Winkler, C. Hu, W.R. Scheidt, F.A. Walker, A.X. Trautwein, J. Am. Chem. Soc. 128 (2006) 1379.
[44] R. Lescouëzec, F. Lloret, M. Julve, J. Vaissermann, M. Verdaguer, Inorg. Chem. 41 (41) (2002) 818.
[45] K.M. Kadish, A.B.P. Lever, H.B. Gray, Iron Porphyrin, Part 2, Chap. 4, Addison-Wesley Publishing Company, Massachusetts, 1983.
[46] M.J.M. Nesset, N.V. Shokhirev, P.D. Enemark, S.E. Ann, F. Walker, Inorg. Chem. 35 (1996) 5188.
[47] K.M. Kadish, C.H. Su, J. Am. Chem. Soc. 105 (1983) 177.